

An Assessment of Broadband Optical Colours as Age Indicators for Star Clusters

M. Hancock^{1*}, B. J. Smith¹, M. L. Giroux¹, and C. Struck²

¹*Department of Physics, Astronomy, and Geology, East Tennessee State University, Box 70652, Johnson City, TN 37614*

²*Department of Physics and Astronomy, Iowa State University, Ames IA 50011*

27 October 2018

ABSTRACT

We present an empirical assessment of the use of broadband optical colours as age indicators for unresolved extragalactic clusters and investigate stochastic sampling effects on integrated colours. We use the integrated properties of Galactic open clusters as models for unresolved extragalactic clusters. The population synthesis code *Starburst99* (Leitherer et al. 1999) and four optical colours were used to estimate how well we can recover the ages of 62 well-studied Galactic open clusters with published ages. We provide a method for estimating the ages of unresolved clusters and for reliably determining the uncertainties in the age estimates. Our results support earlier conclusions based on comparisons to synthetic clusters, namely the (U–B) colour is critical to the estimation of the ages of star forming regions. We compare the observed optical colours with those obtained from *Starburst99* using the published ages and get good agreement. The scatter in the $(B-V)_{observed} - (B-V)_{model}$ is larger for lower luminosity clusters, perhaps due to stochastic effects.

Key words: open clusters and associations: general — galaxies: star clusters — galaxies: stellar content — methods: data analysis

1 INTRODUCTION

Thousands of luminous young star clusters have been discovered in external galaxies by the Hubble Space Telescope (HST) (e.g., Holtzman et al. 1992, 1996; Whitmore et al. 1993; Whitmore & Schweizer 1995; Meurer et al. 1995; Johnson et al. 1999; Benedict et al. 2002; Keel & Borne 2003; Hancock et al. 2003; Whitmore 2003; Weistrop et al. 2004, and references therein). Population synthesis analyses show that these clusters are sometimes very young, with ages of a few to a few tens of Myr. Such age information can be extremely valuable, because it provides clues to cluster formation processes as well as cluster destruction mechanisms. A radial gradient in the ages of clusters within a galaxy can tell us about gas inflow driven by a bar or an interaction. For interacting galaxies, comparison of cluster ages with dynamical models can provide information about star forming mechanisms. For example, gas compression along the Arp 107 tidal arm may have caused a gradient of ages along the arm (e.g., Smith et al. 2005a), while in M51, a burst of cluster formation occurred at around the time of the latest passage of the companion (Bastian et al. 2005; Lee, Chandar, & Whitmore 2005). Cluster synthesis studies have led to the suggestion that there is a high ‘infant mortality’ in star clusters, with many dissolving within 10 Myr (e.g., Bastian et al. 2005; Fall, Chandar, & Whitmore 2005). Star

clusters are themselves sometimes clustered into complexes with characteristic radii of ~ 1 kpc (e.g., Zhang, Fall, & Whitmore 2001; Larsen 2004), and the more massive clusters tend to be located near the centre of these complexes, suggesting cluster merging. Accurate age dating of young clusters associated with ‘ultraluminous X-ray sources’ (ULXs) can help distinguish between stellar-mass and intermediate-mass (100–1000 M_{\odot}) black holes for the origin of the X-ray emission (e.g., Smith et al. 2005b).

Stellar population synthesis models have evolved dramatically in the last several decades, since the pioneering works where data on globular clusters and individual giant stars were used to fill gaps in the evolutionary tracks to make early colour models (e.g. Tinsley 1968, 1972; Struck-Marcell & Tinsley 1978). Recently, several groups have introduced evolutionary synthesis codes, e.g., Bruzual & Charlot (1993) (B&C), Fritze-v. Alvensleben & Gerhard (1994) (GALEV), Fioc & Rocca-Volmerange (1997) (PEGASE), and Leitherer et al. (1999) (*Starburst99*). These new models vary in terms of their input physics, stellar spectral libraries and extinction laws. In general, however, there is good agreement among these models (e.g., Charlot, Worthey, & Bressan 1996; Vázquez & Leitherer 2005).

Unfortunately, however, at the present time, it is not clear how accurate age estimates based on these models are for unresolved extragalactic clusters. In most cases spectra of the targets are not available, so the amount of extinction and metal abundance are unknown. In these cases, one typically compares some combination of UV, optical, and/or near-IR broadband colours to

* E-mail: hancockm@etu.edu (MH); smithbj@etsu.edu (BJS); girouxm@etsu.edu (MLG); curt@iastate.edu (CS)

model cluster spectral energy distributions (SED) to simultaneously estimate age and extinction assuming some metallicity (e.g. Pasquali, de Grijs, & Gallagher 2003; Hancock et al. 2003, 2007; Smith et al. 2008).

There are several parameters that can affect the colour of a cluster other than age. Reddening plays a very important role, as does the chemical composition. However, in some age ranges and colours, reddening and chemical composition are degenerate with age. Furthermore, for low mass clusters ($\lesssim 10^5 M_{\odot}$), the observed integrated colours can be affected by stochastic sampling of the initial mass function (IMF) (see for example, Cerviño & Luridiana 2006, 2004; Cerviño & Valls-Gabaud 2003 and references therein). For example, the random addition of a small number of high mass stars will affect the integrated colour of a cluster. This suggests that the observed integrated colours of low mass clusters may not be good indicators of age when compared to the integrated colours of a stellar population model with a fully sampled IMF.

It is not clear how well a particular set of colours can predict the age of a cluster. Are some colour sets better suited than others? What uncertainties can be expected because of the choice of colours in the comparison? What uncertainties can be expected because of the assumptions made in generating the model SEDs?

Several authors have investigated the use of broadband colours as age indicators by comparison of model colours to the colours of synthetic clusters (e.g. Gil de Paz & Madore 2002; Anders et al. 2004; de Grijs et al. 2005). We use an alternative method by comparing model colours to the integrated colours of resolved Galactic open clusters (OCs). We compare the published integrated colours of well-studied OCs to a set of population synthesis models. These clusters have published ages previously determined by the turn-off of the zero-age main sequence on the H-R diagram. This work parallels that of Pessev et al. (2008), who do a similar analysis of Magellanic Cloud clusters using both optical and near-IR data.

The present paper is organized as follows. In §2 we describe our sample of OCs. We describe the population synthesis models used in this study in §3 and the data analysis in §4. Predicting the ages of the OCs, predicting the amount of extinction and the effects of metallicity, stochastic sampling effects and cluster dissolution are discussed in §5. Finally, we summarize in §6.

2 THE DATA SAMPLE

We started with the set of Galactic open clusters from the WEBDA¹ (Web Base Données Amas) database operated at the Institute for Astronomy of the University of Vienna (Mermilliod 1995). The WEBDA database contains 379 OCs, with well-determined integrated (U–B), (B–V), (V–R), and (V–I) colours, and colour excesses, as found by several authors (Lata et al. 2002; Battinelli, Brandimarti, & Capuzzo-Dolcetta 1994; Pandey et al. 1989; Spassova & Beav 1985; Sagar, Joshi, & Sinhal 1983; Gray 1965). We then culled the WEBDA sample to include only the sample of well-studied OCs in Paunzen & Netopil (2006), who established a list of 72 open clusters with the most accurate known parameters to serve as a standard table for testing isochrones and stellar models. The age uncertainties in Paunzen & Netopil (2006) were determined by measuring the standard deviation of all the published ages in the literature for each of the OCs.

Not all of the 4 integrated colours were determined for each

of the OCs in the Paunzen & Netopil (2006) standard set. To model observations with unknown dust extinction, we reversed the extinction corrections to the published colours using the published values of E(B–V) and the conversions from E(B–V) to the other colour excesses. We used the conversions in Lata et al. (2002), namely $E(U-B)=0.72 E(B-V)+0.05 E(B-V)^2$, $E(V-R)=0.6 E(B-V)$, and $E(V-I)=1.25 E(B-V)$.

From the standard set we created sub-samples of OCs for each of the 4 optical colours and 10 different combinations of colours. When multiple integrated colour measurements were available, we adopted the most recently determined values. Our final data sets include OCs with mean age uncertainties of 19% and ages ranging from 8 Myr to 8.8 Gyr. The metallicities associated with this sample ranges from [Fe/H] $\sim 1/7$ solar to ~ 2.3 solar.

Unfortunately, the WEBDA database does not give the uncertainties on the total colours for individual OCs. According to Sagar, Joshi, & Sinhal (1983), the maximum uncertainty in the published integrated colours for the WEBDA data set is ± 0.2 mag. One of the sources of uncertainty listed is the error in the reddening. Because we have used the published colour excesses to reverse the extinction corrections, we can neglect the extinction uncertainty in the colours. Removing this from the total uncertainty, assuming it was originally added in quadrature, the maximum uncertainty in colour is ~ 0.14 . We assume that all the measured colours have this maximum uncertainty. This assumption further allows us to make fair comparisons of both the accuracy and precision afforded by each colour in age estimation.

3 THE MODEL CLUSTERS

We used a set of evolutionary synthesis models from the *Starburst99* (SB99) code (Leitherer et al. 1999). We used the new v5.1 code, which includes the Padova asymptotic giant branch (AGB) stellar models (Vázquez & Leitherer 2005). The new version accounts for all stellar phases that contribute to the integrated light of a stellar population with arbitrary age from extreme UV to NIR. Strictly speaking, the Geneva tracks are more appropriate for modeling young clusters, less than 10 Myr, when O stars are present. Most of our sample OCs have ages greater than 100 Myr so for simplicity we only consider models with the Padova tracks.

Our SB99 model spectral energy distributions (SEDs) were generated assuming a Kroupa initial mass function (IMF) (favors high mass stars) (Kroupa 2002) with exponents of 1.3 and 2.3 and mass ranges from 0.1 – 0.5 M_{\odot} and 0.5 – 100 M_{\odot} respectively. We have also assumed instantaneous (single burst) star formation, and solar abundances. It has been demonstrated that adopting different forms of the IMF has a minor impact on optical colours (MacArthur et al. 2004), so we have not explored various IMFs. We also generated models with abundances less than (0.2 \times) and greater than (2.5 \times) solar. The model SEDs were reddened from 0.0 mag to 2.0 mag in 0.02 mag increments using the Cardelli, Clayton, & Mathis (1989) reddening law. Finally, the model SEDs were convolved with the Johnson and Kron-Cousins *UBVRI* filter bandpasses and the broadband optical colours were determined. The models span a range of ages from 1 Myr to 20 Gyr. From 1 Myr to 1 Gyr we used a step size of 1 Myr; from 1.1 to 20 Gyr, the step size was 100 Myr. Because the models will be compared to the integrated colours of resolved stellar populations, only the stellar contributions were included in the SEDs. Nebular emission lines have been shown to be important in the first 10^7 yr

¹ <http://www.univie.ac.at/webda/>

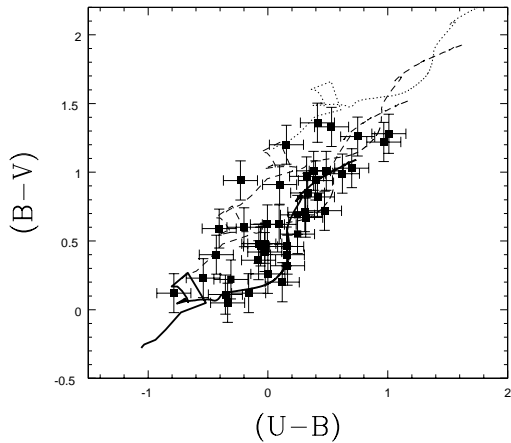


Figure 1. $(B-V)$ vs. $(U-B)$ colour-colour diagram. The black curves are our SB99 models with solar abundances and varying $E(B-V)$. From the bottom to the top, $E(B-V)=0.0$ (thick solid curve), 0.5 (dashed curve), 1.0 (dotted curve), and 1.5 (dotted curve) mags. The filled squares are the observed colours of the standard set of open clusters in the WEBDA sample. For each curve, age increases to the right from 1 Myr to 20 Gyr. Note that we have assumed the maximum uncertainty in colour for each OC.

(Anders & Fritze-v. Alvensleben 2003) and should be considered when studying unresolved stellar populations (see §5.3).

Figure 1 plots the $(B-V)$ vs. $(U-B)$ colour-colour diagram. The black curves are our SB99 models with solar abundances and varying $E(B-V)$. From the bottom to the top, $E(B-V)=0.0$, 0.5, 1.0, and 1.5 mags. The filled squares are the observed colours of the standard set of open clusters in the WEBDA sample. For each curve, age increases to the right from 1 Myr to 20 Gyr. Note that we have assumed the maximum uncertainty in colour for each OC.

4 DATA ANALYSIS

This study is not intended as a test of the SB99 model’s ability to reproduce the colours of young clusters. This has already been demonstrated (see for e.g., Vázquez & Leitherer 2005). We intend to test how well various colours and initial model assumptions can recover the ages of well studied Galactic open clusters. In addition to using the observed colours to estimate ages, we compared the published colours with the model colours calculated assuming the published ages to look for evidence of stochastic sampling effects.

To determine the model predicted ages of the OCs we compared the observed integrated colours to each of the reddened (and unreddened) SB99 model colours, for a single assumed metallicity. We used a χ^2 minimization calculation (e.g., Pasquali, de Grijs, & Gallagher 2003; de Grijs et al. 2005) to determine the best match of the observed colours to the models and hence the ages of the open clusters:

$$\chi^2 = \sum_{i=1}^N \left(\frac{obs_i - model_i}{\sigma_i} \right)^2$$

where N is the number of colours (1-4) used in the analysis, obs_i is the observed colour, $model_i$ is the corresponding model colour, and σ_i is the uncertainty in the obs_i colour. All ages with a fit of $\chi^2 \leq N$ were considered good fits. For each colour set there was therefore

a range of predicted ages for each OC. The age associated with the minimum χ^2 is taken as the best-fit age. To determine the uncertainties in the predicted age we find the minimum and maximum ages within a $\Delta\chi^2$ defined to give a 68% confidence level (e.g., Press et al. 1992). Additionally, we add the model step size to the age uncertainty. We have also predicted the amount of extinction in each case. The amount of extinction applied to the model associated with the best-fit age is the best-fit $E(B-V)$. The uncertainty in the predicted $E(B-V)$ is determined from the minimum and maximum $E(B-V)$ within the same $\Delta\chi^2$ mentioned above. Additionally, we add the model step size to the $E(B-V)$ uncertainty.

In Table 1, we list the subset of our sample that has the U , B , and V magnitudes available. Column one is the name of the OC, column two is the published age, column three is the predicted age determined from the $(U-B)$ and $(B-V)$, column four is M_V , columns five and six are the reddening-corrected measured and zero reddened model $(U-B)$ colours respectively, column seven is the difference of the measured and model $(U-B)$, and columns eight, nine and ten are the same but for the $(B-V)$ colour. It can be seen from Table 1 that for 74% of the OCs, the $(U-B)$ differences are $\lesssim 0.14$, the assumed maximum measurement uncertainty in measured colour, while 60% of the $(B-V)$ differences are $\lesssim 0.14$.

5 RESULTS

5.1 Predicting Ages

In Figure 2, we plot the predicted ages against the published ages, if only $(U-B)$ and $(B-V)$ are used to estimate the ages. We also provide a histogram showing the distribution of the differences between the predicted and published ages, a plot of the predicted $E(B-V)$ s against the published $E(B-V)$ s, and a histogram showing the distribution of the differences between the predicted and published $E(B-V)$ s. In this Figure, we used the solar abundance models. Plots of the predictions determined with the other colour combinations and at other assumed metallicities are similar so are not shown. We see from this figure that with the combination of $(U-B)$ and $(B-V)$ the ages of the OCs can be predicted with reasonable accuracy.

We present Table 2 to discuss both the accuracy and precision of various colours as age indicators. Column one is the colour combination, column two is the number of OCs in the sample with those colours available, and column three is the number of good fits for the solar, 0.2 solar and 2.5 solar models, where the number of good fits is the number of models in our grid that give $\chi^2 \leq N$. Column four is the percentage of recovered ages, which describes how often the predicted age uncertainties overlapped with the uncertainties in the measured ages when solar metallicity is assumed. The results from comparisons to models of 0.2 solar and 2.5 solar abundances are similar so are not shown. Column five lists the average uncertainty in predicted $\log(t)$ in the negative direction for all the OCs, column six lists the average uncertainty in predicted $\log(t)$ in the positive direction for all the OCs, and column seven lists the average of the positive and negative uncertainties for all the OCs. It should be noted that the model ages range from a $\log(t)$ of 6 to 10.3, therefore 2.15 is the maximum mean positive and negative uncertainty in $\log(t)$. Columns eight, nine, and ten are the percentages of predicted ages that are within a factor of 3 of the published ages for the solar abundance model, the 0.2 solar abundance model, and the 2.5 solar abundance model, respectively. This percentage is determined for the best-fit ages without consideration of the pre-

Table 1. Ages and Colour Differences

Name	Age ¹ (pub)	Age ² (pred)	M _V	(U–B) measured	(U–B) model	diff.	(B–V) measured	(B–V) model	diff.
Bochum 10	8±2	1 ⁺³¹ ₋₀	-6.52	-1.05	-0.67	-0.38	-0.24	0.27	-0.51
NGC 6871	9±2	23 ⁺⁶⁰ ₋₂₂	-7.28	-0.89	-0.80	-0.09	-0.24	0.17	-0.41
Stock 14	10±2	31 ⁺⁵⁶ ₋₃₀	-8.25	-0.39	-0.76	0.37	0.34	0.17	0.17
King 12	11±1	13 ⁺⁶⁷ ₋₁₂	-4.90	-0.88	-0.72	-0.16	-0.20	0.14	-0.34
IC 2581	13±3	120 ⁺⁹⁸⁰ ₋₁₁₄	-8.11	-0.33	-0.67	0.34	0.07	0.05	0.02
NGC 3105	21±3	4 ⁺⁴⁹ ₋₃	-6.95	-0.69	-0.67	-0.02	0.11	0.06	0.05
NGC 6250	22±5	66 ⁺¹⁵⁷ ₋₆₁	-4.69	-0.59	-0.66	0.07	-0.16	0.06	-0.22
NGC 6396	30±8	38 ⁺²⁸⁶² ₋₃₇	-5.03	-0.64	-0.58	-0.06	-0.05	0.07	-0.12
Trumpler 1	30±6	11 ⁺²⁹ ₋₁₀	-5.65	-0.88	-0.58	-0.30	-0.04	0.07	-0.11
Lynga 6	35±9	30 ⁺¹⁰³ ₋₂₉	-4.38	-0.65	-0.54	-0.11	0.01	0.07	-0.06
Melotte 20	43±18	82 ⁺¹¹⁴ ₋₇₇	-5.71	-0.42	-0.48	0.06	0.02	0.07	-0.05
King 10	45±11	106 ⁺¹⁰⁵⁹⁴ ₋₁₀₀	-5.34	-0.58	-0.47	-0.11	-0.19	0.07	-0.26
NGC 129	62±15	9 ⁺²⁰ ₋₈	-6.03	-0.64	-0.40	-0.24	0.39	0.09	0.30
NGC 6834	65±18	131 ⁺¹²⁶⁹ ₋₁₂₅	-6.20	-0.45	-0.39	-0.06	-0.10	0.10	-0.20
NGC 6405	71±21	181 ⁺¹⁴⁶ ₋₁₃₄	-3.65	-0.27	-0.38	0.11	-0.03	0.11	-0.14
Collinder 394	74±6	97 ⁺¹⁷⁸ ₋₉₁	-4.74	-0.26	-0.38	0.12	0.23	0.11	0.12
NGC 6025	74±22	82 ⁺¹²¹ ₋₇₆	-4.38	-0.46	-0.38	-0.08	-0.12	0.11	-0.23
NGC 5662	77±20	78 ⁺¹²²² ₋₇₃	-4.38	-0.24	-0.37	0.13	0.30	0.11	0.19
NGC 6087	78±19	143 ⁺³⁰⁹ ₋₁₃₇	-5.09	-0.21	-0.37	0.16	0.18	0.12	0.06
NGC 1778	129±29	149 ⁺⁶⁵⁹ ₋₁₄₃	-4.16	-0.27	-0.25	-0.02	0.09	0.14	-0.05
NGC 1647	130±25	111 ⁺¹⁹⁷ ₋₁₀₅	-2.35	-0.35	-0.25	-0.10	0.07	0.14	-0.07
NGC 5316	166±33	119 ⁺¹²⁶⁸¹ ₋₁₁₃	-4.91	0.13	-0.19	0.32	0.67	0.15	0.52
NGC 744	184±49	256 ⁺¹⁰⁴⁴ ₋₁₇₀	-5.17	-0.14	-0.16	0.02	0.06	0.15	-0.09
Melotte 105	224±53	281 ⁺¹¹¹⁹ ₋₁₈₃	-4.27	-0.11	-0.10	-0.01	0.07	0.16	-0.09
NGC 3532	262±46	243 ⁺³⁶³ ₋₁₆₃	-5.50	-0.03	-0.04	0.01	0.22	0.18	0.04
NGC 2548	364±102	486 ⁺⁴¹¹ ₋₃₄₁	-3.23	0.12	0.07	0.05	0.26	0.23	0.03
Melotte 111	522±82	384 ⁺²⁷³ ₋₂₁₇	-1.95	0.12	0.16	-0.04	0.20	0.33	-0.13
NGC 2527	619±163	317 ⁺⁷⁸³ ₋₂₀₄	-1.90	0.09	0.18	-0.09	0.30	0.39	-0.09
NGC 2266	736±77	498 ⁺¹³⁰² ₋₃₄₈	-3.83	0.40	0.18	0.22	0.62	0.46	0.16
Berkeley 2	794±1	999 ⁺¹⁹¹⁰¹ ₋₉₅₃	-4.18	0.14	0.17	-0.03	0.46	0.49	-0.03
NGC 2355	833±137	238 ⁺³⁵⁶² ₋₁₈₇	-3.67	0.22	0.17	0.05	0.59	0.51	0.08
Berkeley 69	867±48	506 ⁺¹⁹⁵⁹⁴ ₋₃₇₃	-3.16	0.21	0.17	0.04	0.38	0.52	-0.14
NGC 2477	875±238	250 ⁺¹⁰³⁵⁰ ₋₁₈₀	-5.70	0.17	0.17	0.00	0.49	0.53	-0.04
NGC 2192	1072±48	1000 ⁺²²⁰⁰ ₋₉₅₆	-3.53	0.10	0.17	-0.07	0.49	0.62	-0.13
NGC 2660	1351±291	694 ⁺¹⁹⁴⁰⁶ ₋₅₈₅	-4.08	0.34	0.22	0.12	0.61	0.72	-0.11
NGC 1798	1421±16	47 ⁺⁹⁶⁵³ ₋₄₄	-4.86	0.15	0.25	-0.10	0.82	0.77	0.05
NGC 2506	1648±485	259 ⁺²⁹⁴¹ ₋₁₇₅	-4.31	0.22	0.28	-0.06	0.54	0.82	-0.28
NGC 7044	1824±361	19999 ⁺¹⁰² ₋₁₉₈₁₀	-3.93	0.48	0.26	0.22	0.58	0.81	-0.23
Berkeley 32	3477±698	4100 ⁺⁸⁶⁰⁰ ₋₄₀₉₄	-2.97	0.28	0.36	-0.08	0.78	0.91	-0.13
NGC 6253	3949±1086	6800 ⁺¹⁰³⁹⁹ ₋₆₇₉₄	-2.68	0.34	0.38	-0.04	0.81	0.92	-0.11
NGC 2682	4093±958	1300 ⁺⁸²⁰⁰ ₋₁₂₉₄	-3.16	0.28	0.38	-0.10	0.78	0.92	-0.14
NGC 6791	7850±2026	19999 ⁺¹⁰² ₋₁₉₈₀₅	-4.14	0.82	0.46	0.36	1.02	0.97	0.05

¹ Ages in Myr from Paunzen & Netopil (2006)² Ages in Myr predicted from (U–B) and (B–V)

dicted or measured age uncertainties. Unfortunately, the only samples of OCs large enough to draw any significant interpretations are the (U–B), (B–V) and (U–B) and (B–V). Results from the other combinations of colours are merely suggestive.

We see from Table 2 that for several colour combinations the uncertainties in predicted age are relatively large. This is because we have assumed the maximum uncertainty in measured colours for the OCs. Using the actual uncertainties in integrated colours for this sample would not change the predicted ages but would result in better age constraints. Unfortunately the uncertainties in inte-

grated colours of each of these OCs are not available. However, the relative predicted age uncertainties provide a good measure of the precision afforded by each colour and colour combination for age-dating. Looking at the mean uncertainties (column 7 in Table 2) we see that the precision is improved when the (U–B) colour is included.

We see from this table that by using the (U–B) and (B–V) colours up to 83% of the predictions are within a factor of 3 of the published values. For the best-fit (U–B), (B–V), and (U–B) and (B–V) samples, we have determined the differences between the

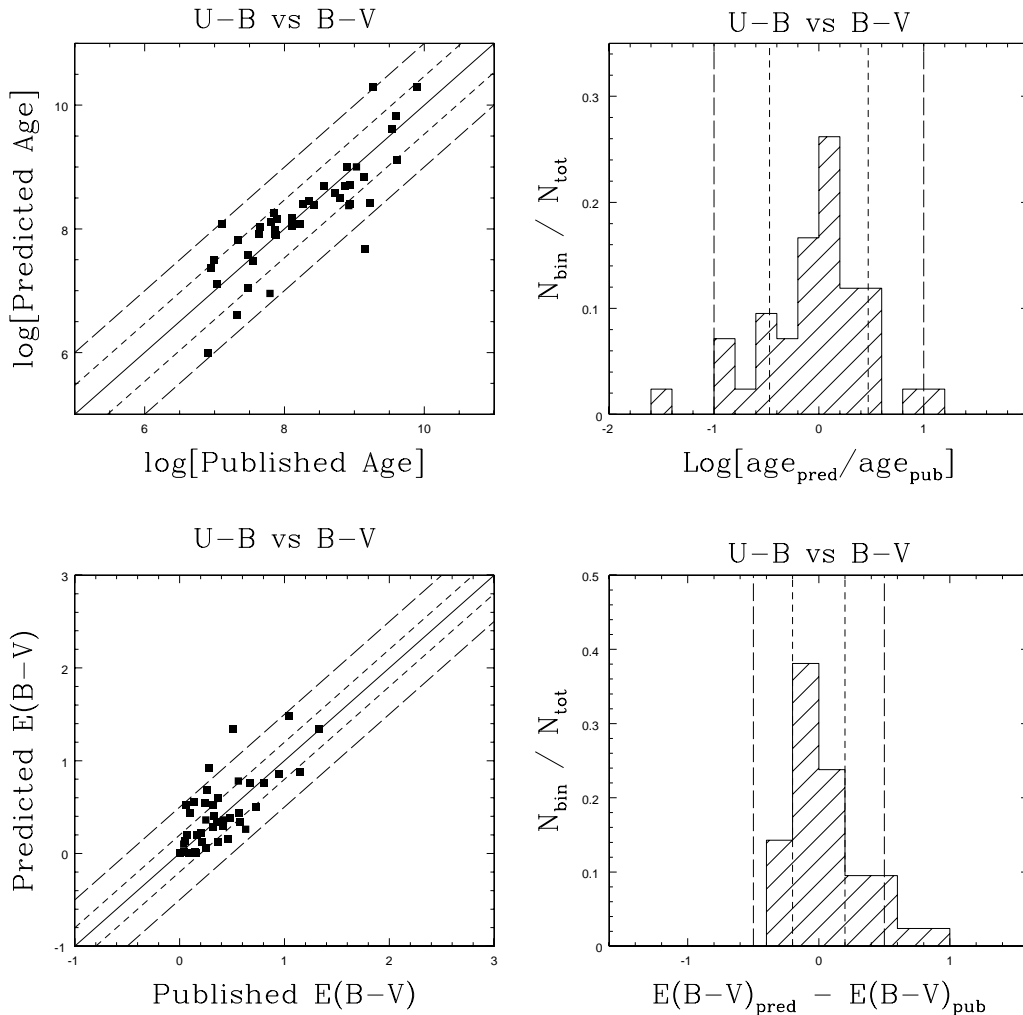


Figure 2. Top Left: Model predicted age versus the published age of the OCs in the WEBDA sample, as determined by the (U–B) vs. (B–V) colours. The solid black line is $y=x$, the inner dashed lines represent a factor of 3 difference in age, and the outer long-dashed lines represent a factor of 10 difference in age. Top Right: Histogram showing the distribution of the difference between the predicted and published ages. The inner and outer dashed lines represent a factor of 3 and 10 change in age respectively. Bottom Left: Model predicted extinction vs. published extinction. The solid black line is $y=x$, the inner dashed lines represent a change of 0.2 mag, and the outer long-dashed line represents a change of 0.5 mag. Bottom Right: Histogram showing the distribution of the difference between the predicted and published $E(B-V)$. The inner and outer dashed lines represent a change of 0.2 and 0.5 mag respectively.

best-fit predicted and measured log ages. We find that 68% of the differences are less than 0.77 dex, 0.86 dex, and 0.44 dex for the (U–B), (B–V), and (U–B) and (B–V) samples respectively. This indicates that (U–B) alone gives more accurate ages than (B–V) alone. We also see that combining (U–B) with (B–V) further improves the accuracy of the predicted ages.

Table 2 shows the importance of the (U–B) colour in measuring the age of a cluster. To the extent that our sample size allows such comparisons, combinations of colours that include (U–B) tend to have more accurate and more precise age predictions. The fact that single colours do not do a good job of constraining the ages is likely because there are three degenerate unknowns, age, reddening, and metallicity, and two filters are not enough to break these degeneracies. This is consistent with results from Anders et al. (2004). However, the (U–B) colour alone is a better predictor of age than any combination of colours that do not include (U–B), regardless of the assumptions about metallicity, consistent with re-

sults from Gil de Paz & Madore (2002) and Anders et al. (2004). The (U–B) colour reflects the contributions from the young and intermediate age stars. Tracing the younger stars in a population is critical to constrain the age. Colours that do not include U only follow the slower-evolving stars and are not as sensitive to changes in age.

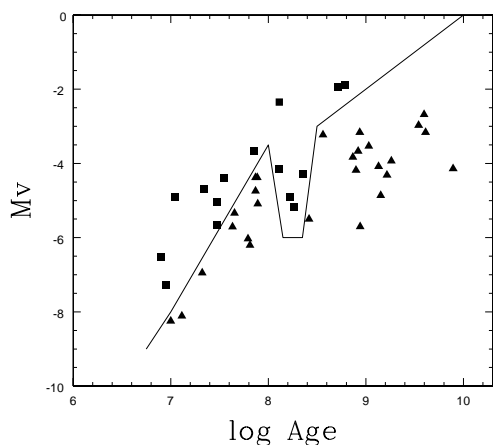
5.2 Extinction and Metallicity

The extinction is predicted well by the same colours that predict the age well. For example, using the (U–B) and (B–V) colours we find that 62% of the $E(B-V)$ estimates are within 0.2 mag of the published values. The colour that is the most sensitive to age, (U–B), is once again critical.

We get similar numbers of good fits to the cluster ages whether we assume 0.2 solar, solar, or 2.5 solar abundances (see Table 2). This implies that, at least within the metallicity range of our sample

Table 2. Prediction Quality

Colours Used	OCs	Good Fits ¹	Rec. Ages ²	Unc down ²	Unc up ²	Unc mean ²	w/in 3 σ	w/in 3 σ	w/in 3 σ
							\odot	0.2 \odot	2.5 \odot
U–B	44	44/44/44	98%	1.03	2.08	1.56	45%	57%	59%
B–V	62	62/62/62	100%	1.18	2.42	1.80	45%	45%	42%
V–R	6	6/6/6	100%	1.37	2.87	2.12	33%	17%	50%
V–I	15	15/15/15	100%	1.40	2.61	2.01	47%	27%	40%
U–B B–V	42	42/42/42	98%	0.84	1.14	0.99	83%	69%	74%
U–B V–R	5	5/4/5	100%	1.33	1.48	1.40	20%	25%	20%
U–B V–I	11	11/8/11	100%	0.75	1.07	0.91	45%	62%	45%
B–V V–R	6	6/6/6	100%	1.26	2.89	2.07	17%	17%	17%
B–V V–I	15	15/15/15	87%	0.69	2.89	1.79	67%	13%	60%
V–R V–I	5	4/4/5	100%	0.59	3.50	2.05	75%	25%	60%
U–B B–V V–R	5	5/5/5	100%	1.16	1.65	1.40	0%	80%	20%
U–B B–V V–I	11	10/7/11	100%	0.63	1.22	0.93	60%	57%	55%
B–V V–R V–I	5	4/4/5	100%	0.36	3.72	2.04	50%	0%	40%
U–B B–V V–R V–I	4	3/2/3	100%	0.39	1.46	0.93	67%	50%	67%

¹ solar/0.2 solar/2.5 solar² solar metallicity assumed**Figure 3.** Published M_V plotted against the published ages of the open clusters in our sample. The curve approximates the lowest luminosity limit curve in Cerviño & Luridiana (2004). The filled black squares are the OCs fainter than the curve while the filled black triangles are brighter.

OCs, knowing the metallicity is not critical for getting a reasonable fit to the cluster age. Note that we are not fitting for the metallicities of these clusters, but instead are testing to see how well we can recover the correct ages and extinctions with standard solar and near solar metallicity models.

5.3 The Effect of $H\alpha$

The SB99 model colours do not include nebular $H\alpha$ emission. This does not impact our analysis of the integrated colours of the OCs because the stellar components are resolved and no $H\alpha$ is included in either the models or the data. However, this should be considered when models are compared to young unresolved clusters in other galaxies.

For clusters younger than ~ 10 Myr, the $H\alpha$ emission con-

tributes significantly to the Johnson R band and minimally to the Johnson V band. From SB99, it is seen that a 1 Myr model has an $EW(H\alpha)$ of ~ 2500 Å, a 5 Myr model has an $EW(H\alpha)$ of ~ 400 Å, and by 10 Myr the $EW(H\alpha)$ is ~ 10 Å. For comparisons to young unresolved clusters, $H\alpha$ emission should be included in the model SEDs. For a discussion about adding $H\alpha$ emission to models to compare to the clusters in Arp 285, see Smith et al. (2008).

5.4 The Effect of Stochastic Sampling of the IMF

It has been shown that traditional synthesis models usually return the mean value of the integrated stellar population distribution (e.g. Cerviño & Luridiana 2006; Luridiana & Cerviño 2007). While this is correct on average, it is not necessarily correct in individual cases because the mean may not be representative of the actual values. Galactic open clusters are typically low mass so will be subject to the effects of stochastic sampling of the IMF (e.g. Cerviño & Valls-Gabaud 2003).

Cerviño & Luridiana (2004) define the lowest luminosity limit as a criterion that must be met in order to compare an observed cluster to a model cluster. The total luminosity of the observed cluster must be larger than the individual contribution of any of the stars in the model. According to Cerviño & Luridiana (2004), clusters brighter than this limit may or may not have a well-sampled IMF, but clusters fainter than this limit will be misrepresented by synthesis models.

Figure 3 is a plot of the published M_V plotted against the published ages of the OCs in our sample. The curve approximates the lowest luminosity limit curve in Cerviño & Luridiana (2004). The filled squares are the OCs fainter than the curve, while the filled triangles are OCs that are brighter. There are 15 OCs fainter and 27 OCs brighter than the curve. From this figure it can be seen that several of the OCs in our sample are brighter than the lowest luminosity limit, but the majority are fainter. This suggests that many clusters in our sample (those fainter) should show these stochastic effects, while several might not (those brighter).

Figure 4 shows the distributions of the differences between the published and the model (U–B) colours and the published and model (B–V) colours for the OCs in our sample. The measured

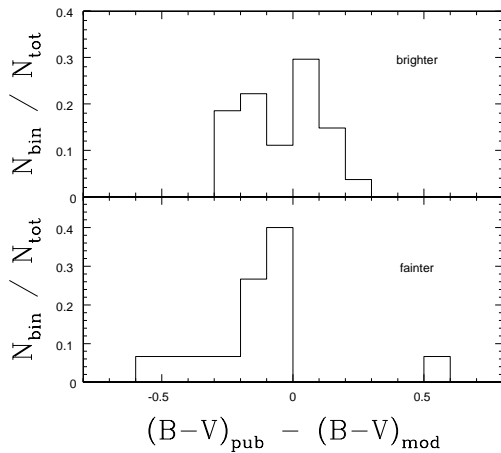
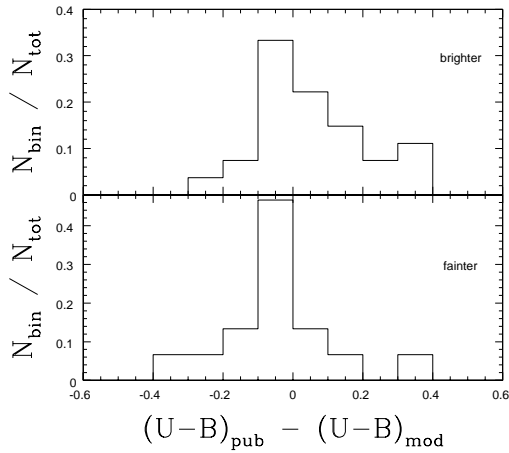


Figure 4. Top: Distribution of the difference between the published $(U-B)_{pub}$ and the model $(U-B)_{mod}$ for the open clusters in our sample. The model colours assume the published ages. The colours are reddening-corrected. The histograms are divided into two groups; fainter than and brighter than the lowest luminosity limit curve, as shown in Figure 3. Bottom: Same as above but for the $(B-V)$ colours.

colours are reddening-corrected. The model colours assume the published ages. To make comparisons, only OCs with both integrated $(U-B)$ and $(B-V)$ colours are included in these distributions. The histograms are divided into 2 groups, those brighter and those fainter than the lowest luminosity curve, as in Figure 3.

For the $(U-B)$ colour, a Kolmogorov-Smirnov (K-S) test cannot rule out that the brighter and fainter samples originated from the same parent distributions. The rms for the differences in $(U-B)$ are 0.16 and 0.17 for the brighter and fainter samples respectively. However, for $(B-V)$, a K-S test suggests a probability of only 0.012 that the two samples (brighter and fainter) originate from the same parent distribution. The rms values are 0.15 and 0.25 for the $(B-V)$ distributions respectively. The scatter appears slightly larger for the fainter samples, with the $(B-V)$ difference being slightly skewed to negative numbers (see Figure 4).

Figure 5 shows the differences between the published and model $(U-B)$ and $(B-V)$ colours plotted against the published ages using the same sample as in Figure 4. The measured colours

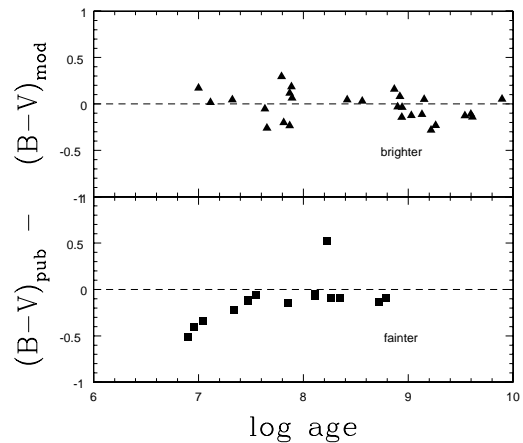
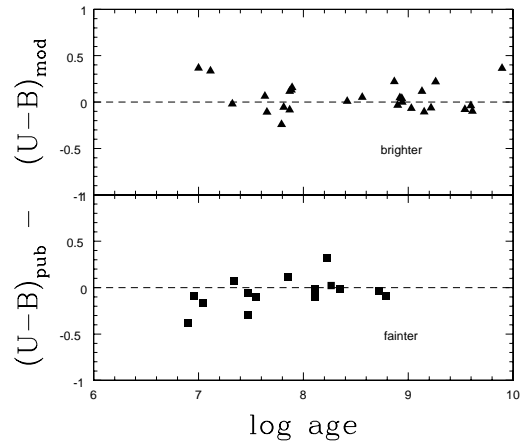


Figure 5. Top: Difference between the published and model $(U-B)$ colours against the published ages of the clusters. Bottom: Difference between the published and model $(B-V)$ colours against the published ages of the clusters. The two panels describe the same two groups as above. The dashed lines show zero colour difference.

are reddening-corrected. For each colour difference the OCs are divided into the same bins as described above. From Figure 5 it can be seen that the scatter in the $(U-B)$ colour differences do not appear to be correlated with age. The fainter $(B-V)$ difference sample appears to have a slight dependence on age in that the published $(B-V)$ colours are bluer than the model colours for the younger OCs, consistent with results in Bruzual (2002) (see below). Given this, the K-S results, and the larger rms, we might be seeing stochastic sampling effects in the differences between the measured and model $(B-V)$ colours.

In Figure 6, we plot the published reddening-corrected $(U-B)$ colour against the published reddening-corrected $(B-V)$ colour for our OCs. This figure is divided into the same two groups described above. Also on this figure are our SB99 models with $E(B-V)$ of 0.0 mag (solid curve) and 0.5 mag (dashed curve). This figure shows that the scatter of these colours around the models is not a function of M_V . Note that relatively young clusters (that is, blue clusters) tend to lie above and to the left of the zero extinction model curve.

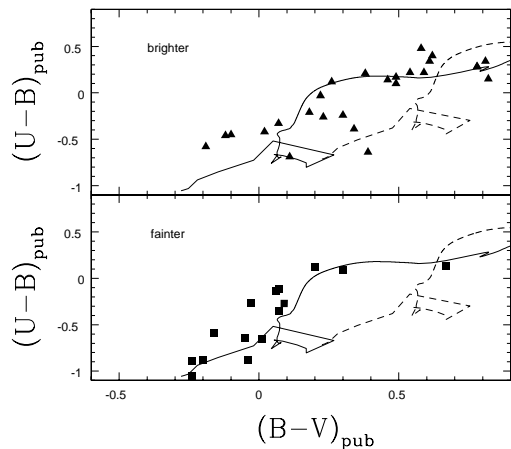


Figure 6. Published $(U-B)$ against published $(B-V)$ for the OCs. The figures are divided into 2 groups as described above. The curves are our SB99 models with $E(B-V)$ of 0.0 mag (solid curve) and 0.5 mag (dashed curve).

Figures 4 and 5 show that this is predominately due to the fainter clusters being bluer in $(B-V)$ than the models.

Our results can be compared to population synthesis studies that explicitly investigate stochastic effects. For example, Bruzual (2002) and Bruzual & Charlot (2003) have run Monte Carlo simulations of low mass star clusters, to investigate how stochastic effects can cause observed colours to differ from models with full-sampled IMFs. In their simulations, young model clusters with masses of $10^3 M_{\odot}$ also lie above models with fully-sampled IMFs on a $(U-B)$ vs. $(B-V)$ plot (Bruzual 2002), consistent with what we see in Figure 6. Thus at least some of the observed scatter may be due to stochastic effects.

From these figures and tables we see suggestive evidence of stochastic sampling of the cluster IMF in this sample of OCs. It is possible that the uncertainties in the measured colours and/or ages are large enough (0.14 mag and 19% respectively) that the effects of stochastic sampling are washed out. However, figure 1 in Cerviño & Valls-Gabaud (2003) shows that the expected scatter in the integrated $(B-V)$ of a 10 Myr cluster with 10^3 or less stars is much larger than our assumed colour uncertainties. Most of the OCs in our sample are much older than 10 Myr. It is possible that stochastic sampling effects are smaller in $(B-V)$ for older clusters. After ~ 10 Myr the most luminous stars will have evolved off of the main sequence and will contribute more strongly to the red end of the integrated cluster SED. de Grijs et al. (2005) remark that stochastic sampling effects affect broadband photometry to a smaller extent than spectroscopy. In a follow up paper (Hancock et al., in prep.) we will explore a more detailed analysis of the stellar content of these resolved OCs to further investigate the extent to which stochastic sampling of the IMF affects the integrated broadband colours. If stochastic sampling effects are observationally characterized in this sample of OCs, they will provide a good bench mark for testing future population synthesis models.

5.5 The Effect of Cluster Dissolution

Current stellar population synthesis models do not take into account the effects of cluster dissolution. Mass segregation causes

the massive stars to concentrate towards the centre of a cluster while the low-mass stars tend to populate the outer regions. A consequence of mass segregation is that low-mass stars tend to be preferentially ejected from star clusters. The mass function (MF) therefore changes drastically during the evolution of a cluster, as a consequence, becoming less steep than the IMF (e.g. Baumgardt & Makino 2003). The preferential loss of low-mass stars will change the integrated colours of a cluster (e.g. Lamers, Anders, & de Grijs 2006). Such a time evolution of the integrated colours resulting from cluster dissolution can be difficult to disentangle from stellar evolutionary effects.

The colour change of a star cluster due to dissolution depends upon its age, its mass, and its dissolution time scale (t_{dis}), with the effect being larger for later ages and longer t_{dis} . Lamers, Anders, & de Grijs (2006) show that, for a $10^5 M_{\odot}$ cluster, the $(B-V)$, $(V-I)$ and $(V-K)$ colours are not significantly affected by the preferential loss of low-mass stars during the first 80% of their t_{dis} , with $\Delta(V-I) = 0.03$ and 0.1 mag for a t_{dis} of 1 Gyr and 10 Gyr respectively. However, in the last 20% of a cluster's life, the colour effect can be quite large, up to $\Delta(V-I) = 0.3$ mag.

Our sample clusters likely have masses between 10^3 and $10^4 M_{\odot}$. This implies t_{dis} between ~ 100 Myr and 2 Gyr (Lamers & Gieles 2006). Given that 45% of our sample have ages less than 80 Myr and 86% have ages less than 1.6 Gyr (see Table 1), it is likely that most of our clusters are not in the last 20% of their lifetimes, but we can not rule out the possibility that some might be near the end of their lifetimes. Thus the effect of dissolution on their colours is likely small, typically smaller than our assumed uncertainties of 0.14 magnitudes.

Using the stellar data available on WEBDA for a sample of our OCs covering a representative range of distances, we found that $\sim 85\%$ contained stars $\lesssim 0.5 M_{\odot}$. To determine the effects that low mass stars have on the model integrated colours we compared Kroupa models with lower mass cutoff of $0.1 M_{\odot}$ with those with $0.5 M_{\odot}$. We found no significant differences in the $(U-B)$, $(B-V)$, $(V-R)$, or $(V-I)$ colours.

6 SUMMARY

We present an empirical assessment of the use of broadband colours as age indicators for unresolved extragalactic clusters and investigate stochastic sampling effects on integrated colours. The population synthesis code *Starburst99* (Leitherer et al. 1999) and four optical colours were used to estimate how well we can recover the ages of 62 well-studied Galactic open clusters with published ages. We conclude the following:

1) Galactic open clusters can be used for testing the integrated properties from population synthesis and serve as reasonable benchmarks for future assessments of age-dating methods.

2) The $(U-B)$ colour is critical. Only colour combinations that included $(U-B)$ resulted in good age and extinction predictions, consistent with previous results.

3) Only with $(U-B)$ included were the predicted age uncertainties reasonably constrained.

4) Changes of a factor of ~ 2 in assumed metal abundance do not result in significantly different predictions of cluster age. This indicates that the uncertainties in predicting the age of a cluster resulting from the age-reddening degeneracy dominate over the other sources of degeneracy in these optical bands, over our age range and metallicity range. Another possibility is that uncertain-

ties in the measured colours (and hence the predicted ages) dwarf the metallicity-age degeneracy.

5) A χ^2 minimization and a $\Delta\chi^2$ defined to give 68% confidence levels provide reliable age estimates, and more importantly, reliable age uncertainties. The difference in the photometric ages and the ages derived from the HR-diagrams of our selected cluster sample with both the (U–B) and (B–V) colours are smaller than 0.5 dex for 79% of the clusters, with a maximum difference of 1.5 dex.

6) It is likely that the uncertainties in the measured colours and/or ages are large enough (0.14 mag and $\sim 20\%$ respectively) that the effects of stochastic sampling are washed out. A more detailed analysis of the stellar content of these resolved OCs will be required to further investigate the extent to which stochastic sampling of the IMF affects the integrated broadband colours.

7) If stochastic sampling effects are observationally characterized in this sample of OCs, they will provide a good bench mark for testing future population synthesis models.

ACKNOWLEDGMENTS

We thank the anonymous referee for his/her helpful comments and suggestions. This research has made use of the WEBDA database, operated at the Institute for Astronomy of the University of Vienna. The authors would like to thank Ernst Paunzen for providing ASCII tables of the WEBDA data. The authors also thank Alessandra Stone for help with the data acquisition. This work has been supported by the NASA LTSA grant NAG5-13079.

REFERENCES

Anders P., Bissantz N., Fritze-v. Alvensleben U., de Grijs R. 2004, MNRAS, 347,196
 Anders P., Fritze-v. Alvensleben U. 2003, A&A, 2003, 401, 1063
 Bastian N., Gieles M., Efremov Y. N., Lamers H. J. G. L. M. 2005, A&A, 443, 79
 Battinelli P., Brandimarti A., Capuzzo-Dolcetta R. 1994, A&AS, 104, 379
 Baumgardt H., Makino J. 2003, MNRAS, 340, 227
 Benedict G. F., Howell D. A., Jørgensen I., Kenney J. D. P., Smith B. J. 2002, AJ, 123, 1411
 Bruzual A. G., Charlot S. 2003, MNRAS, 344, 1000
 Bruzual A. G. 2002, in IAU Symp. Ser. 207, Extragalactic Star Clusters, ed. D. Geisler, E. K. Grebel, & D. Minniti, 616
 Bruzual A. G., Charlot S. 1993, ApJ, 405, 538
 Cardelli J. A., Clayton G. C., Mathis J. S. 1989, ApJ, 345, 245
 Cerviño M., Luridiana V. 2006, A&A, 451, 475
 Cerviño M., Luridiana V. 2004, A&A, 413, 145
 Cerviño M., Valls-Gabaud D. 2003, MNRAS, 338, 481
 Charlot S., Worthey G., Bressan A. 1996, ApJ, 457, 625
 de Grijs R., Anders P., Lamers H. J. G. L. M., Bastian N., Fritze-v. Alvensleben U., Parmentier G., Sharina M. E., Yi S. 2005, MNRAS, 359, 874
 Fall S. M., Chandar R., Whitmore B. C. 2005, ApJ, 631, L133
 Fioc M., Rocca-Volmerange B. 1997, A&A, 326, 950
 Fritze-v. Alvensleben U., Gerhard O. E. 1994, A&A, 285, 751
 Gil de Paz A., Madore B. 2002, AJ, 123, 1864
 Gray D.F. 1965, AJ, 70, 362
 Hancock M., Smith B. J., Struck C., Giroux M. L., Appleton P. N., Charmandaris V., Reach W. T. 2007, AJ, 133, 676

Hancock M., Weistrop D., Eggers D., Nelson C. H. 2003, AJ, 125, 1696
 Holtzman J. A. et al. 1992, AJ, 103, 691
 Holtzman J. A. et al. 1996, AJ, 112, 416
 Johnson K. E., Vacca W. D., Leitherer C., Conti P., Lipsy S. J. 1999, AJ, 117, 1708
 Keel W. C., Borne K. D. 2003, AJ, 126, 1227
 Kroupa P. 2002, in ASP Conf. Ser. 285, Modes of Star Formation and the Origin of Field Populations, ed. E. K. Grebel & W. Brandner (San Francisco: ASP), 86
 Lamers H. J. G. L. M., Anders P., de Grijs R. 2006, A&A, 452, 131
 Lamers H. J. G. L. M., Gieles M. 2006, A&A, 455, L17
 Larsen S. S. 2004, A&A, 416, 537
 Lata S., Pandey A.K., Sagar R., Mohan V. 2002, A&A, 388, 158
 Lee M. G., Chandar R., Whitmore B. C. 2005, AJ, 130, 2128
 Leitherer C. et al. 1999, ApJS, 123, 3
 Luridiana V., Cerviño M. 2007, ASPC, 374, 393
 MacArthur L. A., Courteau S., Bell E. F., Holtzman J. A. 2004, ApJS, 152, 175
 Mermilliod J.-C. 1995, in “Information and On-Line Data in Astronomy”, Eds D. Egret & M.A. Albrecht (Kluwer Academic Press, Dordrecht), p. 127-138
 Meurer G. R., Heckman T. M., Leitherer C., Kinney A., Robert C., Garnett D. R. 1995, AJ, 110, 2665
 Pandey A.K., Bhatt B.C., Mahra H.S., Sagar R. 1989, MNRAS, 236, 263
 Pasquali A., de Grijs R., Gallagher J. S., 2003, MNRAS, 345, 161
 Paunzen E., Netopil M. 2006, MNRAS, 371, 1641
 Pessev P. M., Goudfrooij P., Puzia T. H., Chandar R. 2008, MNRAS, 385, 1535
 Press W. H., Teukolsky S. A., Vetterling W. T., Flannery B. P. 2002, Numerical Recipes in Fortran: the art of scientific computing, 2nd ed. (Cambridge University Press)
 Sagar R., Joshi U.C., Sinhal S.D. 1983, Bull. Astron. Soc. India, 11, 44
 Smith B. J., Struck C., Appleton P. N., Charmandaris V., Reach W., Eitter J. J. 2005, AJ, 130, 2117
 Smith B. J., Struck C., Nowak M. A. 2005b, AJ, 129, 1350
 Smith B. J. et al. 2008, AJ, 135, 2406
 Spassova N.M., Beav P.V. 1985, Astrophys. Space Sci., 112, 111
 Struck-Marcell C., Tinsley B. M. 1978, ApJ, 221, 562
 Tinsley B. M. 1968, ApJ, 151, 547
 Tinsley B. M. 1972, A&A, 20, 383
 Vázquez G. A., Leitherer C. 2005, ApJ, 621, 695
 Weistrop D., Eggers D., Hancock M., Nelson C. H., Bachilla R., Kaiser M. E. 2004, AJ, 127, 1360
 Whitmore B. C. 2003, in Space Telescope Science Inst. Symp. Series 14, A Decade of Hubble Space Telescope Science, ed. M. Livio, K. Noll, & M. Stiavelli (Cambridge: Cambridge Univ. Press), 153
 Whitmore B. C. et al. 1993, AJ, 106, 1365
 Whitmore B. C., Schweizer F. 1995, AJ, 109, 960
 Zhang Q., Fall S. M., Whitmore B. C. 2001, ApJ, 561, 727

This paper has been typeset from a $\text{\TeX}/\text{\LaTeX}$ file prepared by the author.